Online Transmission Line Loadability Assessment Using Synchrophasor Measurements

Jiangmeng Zhang, Alejandro D. Domínguez-García, and Peter W. Sauer
Department of Electrical and Computer Engineering
University of Illinois at Urbana-Champaign Urbana, Illinois 61801
Email: {jzhang67, aledan, psauer}@illinois.edu

***Abstract*—This paper proposes a measurement-based method to assess transmission line loadability, particularly when determined by stability constraints. A power system two-area equivalent model provides the basis for the proposed line loadability assessment method, with the angle across this equivalent model defining a metric of the closeness to the system stability limits. In this paper, using advanced synchrophasor measurements, Kalman filter-based algorithms are applied to estimate the parameters and variables of the aforementioned equivalent system model. A significant benefit of the proposed method is that it does not rely on the knowledge of the system topology and parameter values. The proposed method is illustrated through a two-bus system example and a two-area system case study.**

I. Introduction

Transmission line loadability analysis is a critical component of system planning and operating studies. Line loading margins provide a useful metric to operate the power system to satisfy demands while ensuring a stable operation. Transmission line loading limits are also essential to determine locational marginal prices in power markets. Therefore, the assessment of transmission line loadability under various operating points becomes important. There are three basic factors which limit the loabability of a transmission line: (i) thermal, (ii) voltage drop, and (iii) stability limitations. It is well recognized that the loadability of short lines is principally limited by thermal constraints, medium-length lines by voltage drop limitations, and long lines by stability considerations [1]. While line loading margins determined by thermal and voltage-drop considerations can be directly obtained from equipment thermal ratings and the terminal bus voltage measurements, respectively, those determined by line stability limitations are not as straightforward to obtain. In this paper, we focus on the assessment of transmission line loadability when limited by stability considerations. For subsequent developments, we note that long high-voltage transmission lines (200 miles and above), whose loadability is determined by stability considerations, are usually used to interconnect two areas that are otherwise weakly coupled.

Transmission line loadability has been widely studied (see, e.g., [1]–[3]). For example, the so-called St. Clair curves, which relate line loadability and line length, have been presented based on practical experience in 1953 [1]. The authors in [2] developed an analytical basis to rebuild the St. Clair curves and it was shown that the results, which are derived from a simplified equivalent two-machine representation of the system, and the original St. Clair curve are nearly identical. Furthermore, the authors in [3] extended the analytical basis to operating studies. However, as discussed in [3], it is challenging to adapt the analytical technique to on-line assessment of line loadability, since real-time system state information is required and a further study for obtaining the equivalent system representation is necessary. The deployment of phasor measurement units (PMUs) presents promising potential to address the problem described above. PMUs can directly measure the voltage and current phasors (i.e., both magnitudes and angles), which are referred to as synchrophasor measurements, at a high sampling rate [4].

In this paper, instead of obtaining the equivalent system model from short circuit analyses with system topology information and parameters as in [3], we propose a measurement-based method to obtain the equivalent system model. A major benefit of the proposed method is the elimination of reliance on system topology and parameter information, i.e., only synchrophasor measurements of currents and voltages on the two terminals of the transmission line under consideration are required. Although transmission line stability limitation is assessed in steady state, we rely on small disturbances (such as load and generation variations) inherent to the system in order to estimate the equivalent system based on only the synchrophasor measurements. Specifically, we assume that the response to the aforementioned small disturbances of each of the machines in the equivalent can be captured by the classical machine model, where the internal voltages are assumed to be fixed, consistent with the assumption made in [3]. Furthermore, the effectiveness of this two-area model has been validated in the dynamic system equivalencing literature (see, e.g., [5], [6] and the references therein).

This work extends our earlier work in [7] by casting the problem as a dynamic system estimation problem. The framework developed in this paper integrates two bodies of work; namely synchrophasor measurement-based system equivalencing (see, e.g., [5], [6]) and the Kalman filtering literature (see, e.g., [8]–[11]). The extended Kalman filter and its variants are implemented to address the effect of noise on PMU measurements and to evaluate the equivalent parameters systematically. In addition, our framework also allows for higher-order equivalent system models if necessary. Then, with the estimated equivalent system parameters, transmission line loadability can be assessed.

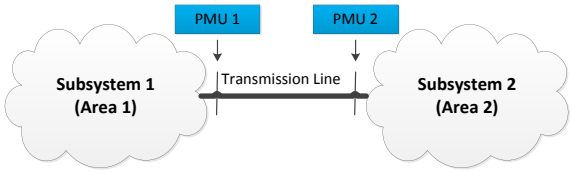

Fig. 1: Two-area power system.

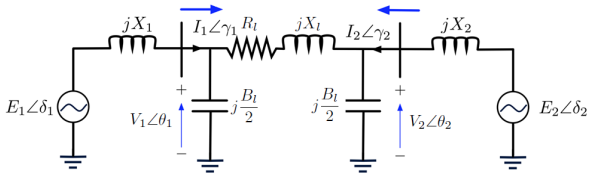

Fig. 2: Two-area power system equivalent model.

II. Problem Formulation and System Model

In this section, we derive the analytical model used to assess transmission line loadability. A metric to describe the loading of the line under consideration is also introduced. We then provide the equivalent system model formulation.

A. Transmission Line Loadability Assessment

Consider a power system, where a transmission line of interest connects two subsystems as shown in Fig. 1. The two subsystems are equivalent to two simplified circuits, while the connecting transmission line is retained in the equivalent system model [2]. As shown in Fig. 2, each equivalent circuit consists of a reactance, respectively denoted by X_1, X_2, and an internal voltage source, respectively denoted by $E_1\angle\delta_1$, $E_2\angle\delta_2$. The transmission line is represented by the so-called π model.

As mentioned in Section I, the work in this paper focuses on quantifying the loadability of long transmission lines, which are dominated by stability considerations. Stability is usually measured in terms of the margin between the current power flowing across the transmission line and the maximum possible power flow $P_{\max}$ as a percentage of $P_{\max}$ [3]; we refer to this margin as stability margin (SM). For the system in Fig. 2, if we neglect the line resistance (which is usually small compared to line reactance) and the shunt admittances, the power flowing across the system is exactly proportional to the sine of the angle across the system (AAS). Therefore, the stability margin, reflecting the line loadability, can be calculated as follows [3]:

$$\text{SM} = \frac{P_{\max} - P}{P_{\max}} = 1 - \sin(|\delta_1 - \delta_2|). \tag{1}$$

We note that the setup of our original system in Fig. 1 can be rationalized by the fact that the long transmission lines are usually used to interconnect two areas that are otherwise weakly coupled. Therefore, the two subsystems in Fig. 1 are not coupled except through the transmission line of interest.

B. Equivalent System Model

As shown in Fig. 1, two PMUs are set up at the terminals of the transmission line under consideration to measure the voltage and current phasors. We denote by $\bar{V}_i = V_i\angle\theta_i$ $(i = 1, 2)$ the voltage phasor at each end of the transmission line, and by $\bar{I}_i = I_i\angle\gamma_i$ $(i = 1, 2)$ the phasors describing the current flowing into the transmission line from each end as shown in Fig. 2. Each of the subsystem equivalent circuits is modeled using a classical machine model, which can generate or consume power [5]. Now the equivalent system can be described by a set of differential-algebraic equations (DAEs) (neglecting resistance and shunt admittances):

$$\frac{\mathrm{d}\delta_1}{\mathrm{d}t} = \omega_1 - \omega_s, \tag{2a}$$

$$\frac{\mathrm{d}\omega_1}{\mathrm{d}t} = \frac{\omega_s}{2H_1}\left(P_{M1} - \frac{E_1E_2\sin(\delta_1 - \delta_2)}{X_1 + X_l + X_2}\right), \tag{2b}$$

$$\frac{\mathrm{d}\delta_2}{\mathrm{d}t} = \omega_2 - \omega_s, \tag{2c}$$

$$\frac{\mathrm{d}\omega_2}{\mathrm{d}t} = \frac{\omega_s}{2H_2}\left(P_{M2} - \frac{E_1E_2\sin(\delta_2 - \delta_1)}{X_1 + X_l + X_2}\right), \tag{2d}$$

$$\bar{V}_1 = \frac{E_1\angle\delta_1(X_l + X_2) + E_2\angle\delta_2X_1}{X_1 + X_l + X_2}, \tag{2e}$$

$$\bar{I}_1 = \frac{E_1\angle\delta_1 - E_2\angle\delta_2}{j(X_1 + X_l + X_2)}, \tag{2f}$$

$$\bar{V}_2 = \frac{E_2\angle\delta_2(X_l + X_1) + E_1\angle\delta_1X_2}{X_1 + X_l + X_2}, \tag{2g}$$

$$\bar{I}_2 = \frac{E_2\angle\delta_2 - E_1\angle\delta_1}{j(X_1 + X_l + X_2)}, \tag{2h}$$

where ω_s is the system nominal frequency, P_{Mi} is the equivalent mechanical power input, ω_i is the speed and H_i is the equivalent inertia for $i = 1, 2$. In this model, equations (2a)-(2d) are referred to as state equations, describing the state evolution, while equations (2e)-(2h) are referred to as observation equations, describing Kirchhoff's relations for the circuit in Fig. 2. In practice, the values of the observations (i.e., the PMU measurements $\bar{V}_i$, $\bar{I}_i$) can be set to be expressed in either polar form or cartesian form. The observation equations then can be converted to scalar equations accordingly.

Define $x{=}[x_1, x_2]^T$, where $x_i{=}[\delta_i, \omega_i, E_i, X_i, H_i, P_{Mi}]^T$, $i{=}1, 2$, and $y^{\text{true}}{=}[V_1, \theta_1, I_1, \gamma_1, V_2, \theta_2, I_2, \gamma_2]^T$. Measurement noise is unavoidable in the system observations; therefore, we assume that the system measurements can be described as $y = y^{\text{true}} + \eta$, where the entries of $\eta \in \mathbb{R}^8$ are independent white noise processes. Then the resulting DAE model can be compactly written as:

$$\dot{x} = \tilde{f}(x), \tag{3a}$$

$$y = h(x) + \eta, \tag{3b}$$

where $\tilde{f} : \mathbb{R}^{12} \mapsto \mathbb{R}^{12}$ and $h : \mathbb{R}^{12} \mapsto \mathbb{R}^8$ can be defined by using (2). Since in the classical model, the internal voltage magnitudes and reactances are assumed to be constant, the derivatives of E_i, X_i, H_i and P_{Mi} $(i = 1, 2)$ are set to zero.

C. Discretized Model

Since PMUs provide measurements at discrete time instants, we utilize a discretized version of (3). Assuming the time step Δt is sufficiently small (in this case, Δt depends on the PMU measurement rate, typically 0.1–0.01 s), the expression in (3b) can be approximated by a nonlinear recursive equation model of the form:

$$x_{k+1} = x_k + \tilde{f}(x_k)\Delta t =: f(x_k),\ k \in \mathbb{Z}^+; \tag{4}$$

then we can rewrite (3) as:

$$x_{k+1} = f(x_k), \tag{5a}$$
$$y_{k+1} = h(x_{k+1}) + \eta_{k+1},\ k \in \mathbb{Z}^+. \tag{5b}$$

Now the problem is to estimate the state x based on the observation y in (3) using the descretized model in (5).

III. Equivalent System Parameter Estimation

In this section, we provide a summary of the key ideas behind Extended Kalman filtering. Then, we propose a modified extended Kalman filter to address the issues that arose when applying extended Kalman filter to our system. Examples are also included to illustrate the ideas presented.

A. Extended Kalman Filter (EKF)

Given the nonlinear model in (5), the first intuitive idea to estimate its state is to apply an extended Kalman filter. As a nonlinear version of the Kalman filter, the core concept behind the extended Kalman filter is the linearization of the system model around the state estimate at each time step. However, the performance of the extended Kalman filter varies significantly depending on the nonlinearity of the system. As a result, the convergence region of the initial estimates may be significantly limited if the system is highly nonlinear, meaning the filter may fail to converge if the initial estimates are away from the correct values; our model has this problem as we will see in Example 1. It is obvious that it is very difficult to precisely know the correct values of the initial states. One way to address this issue is to take a guess of the initial state and set the initial estimate covariance to be a sufficiently large number times the identity matrix; however, this results in the estimates converging to some value that is not the correct one [10]. Therefore, in the next section, we propose the use of a modified iterated extended Kalman filter (see, e.g., [9]).

Example 1: In order to focus on the performance of the filter, we assume that the equivalent on the right of Fig. 1 is an infinite bus, which means $X_2 = 0$ p.u., $E_2 = 1$ p.u., and $\delta_2 = 0$ rad. The parameter values are listed in Table I. Unless otherwise stated, all quantities are in per unit (p.u.). We apply a disturbance to the system, and use an extended Kalman filter to estimate the states δ_1, ω_1, E_1, X_1, H_1, and P_{M1}. The comparisons of the correct values and the estimates of δ_1 with different initial state estimates and estimate covariance are depicted in Fig. 3. As shown in Fig. 3(a), if the initial state estimates are set to the correct values (although this may be difficult in practice), the estimates and the actual state values

TABLE I: Example system parameter values.

E_1	$\delta_1(0)$ [rad.]	X_1	X_l	H [s]	P_{M1}	$\bar{E}_2$
1.02	0.2501	0.2	0.05	4	1	$1\angle 0$

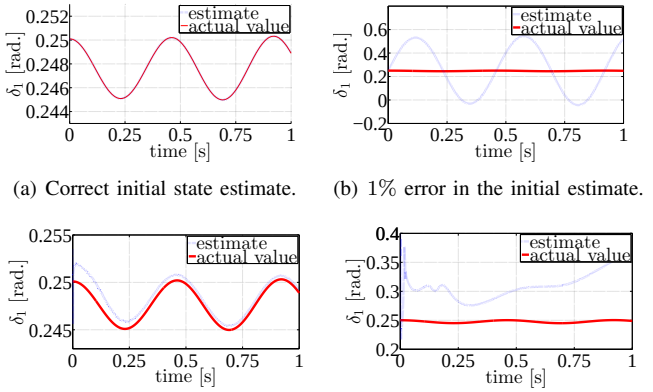

(a) Correct initial state estimate.

(b) 1% error in the initial estimate.

(c) Initial estimate close to the actual values.

(d) Initial state estimate away from the correct values.

Fig. 3: Extended Kalman filter performance.

are nearly equivalent. However, as shown in Fig. 3(b), if the initial state estimates are not the correct values, although very close (1% error in this case), and the estimate covariance is still 0, the resulting state estimates are far from the correct values. As shown in Fig. 3(c), if the initial state estimates are not the correct values (but still close to the correct values) and the estimate covariance are set to be $10^6 I$, where I is the identity matrix, the state estimates converge to biased values, meaning asymptotic convergence error exists. When the initial state estimates are not close to the correct values, the system easily fails to converge due to the system nonlinearity, as shown in Fig. 3(d). By varying the initial state estimates, we found that this problem is particularly severe for the equivalent reactance X_1, which results from the fact that the state evolution function involves a nonlinear inverse function of X_1. As shown in Fig. 3(d), when the initial state estimate of X_1 is set to be 0.4, even with large initial estimate covariance, the estimates diverge. Furthermore, unlike other parameters, such as E_1 which is usually close to 1, it is difficult to guess the range of X_1 initially. ■

B. Modified Iterated Extended Kalman Filter Processing

In the model in (5), both the state dynamic evolution equations and the observation equations are nonlinear. By properly manipulating the observation equations, the system can be decoupled in the senses that (i) the dynamic evolution equations and observations equations are decoupled; and (ii) the two subsystems on the two sides are decoupled as well. To this end, for $i = 1, 2$, we can derive the following relationship:

$$I_i(t)^2 X_i^2 + 2I_i(t)V_i(t)X_i \sin(\theta_i(t) - \gamma_i(t)) + V_i(t)^2 - E_i^2 = 0. \tag{6}$$

In the above expression, no dynamics are included. It is worth noting that this equation also indicates that only the difference between the current phase angle and voltage phase

angle, instead of their absolute values, matters. Therefore the mismatch issue caused by the PMU measuring at the off-nominal frequency will not affect the estimation accuracy here. The details can be found in [4].

Let

$$\tilde{g}_{i,t}(x) = I_i(t)^2 X_i^2 + 2I_i(t)V_i(t)X_i \sin(\theta_i(t) - \gamma_i(t)) + V_i(t)^2; \quad (7)$$

for two sets of measurements at time t and $t-T$, we can further derive the following relationship:

$$\tilde{g}_{i,t}(x) - \tilde{g}_{i,t-T}(x) = 0 \quad (8)$$

where T is a constant time interval. In practice, T should be a multiple of the time step Δt. Now, the system of interest becomes a nonlinear algebraic equation model of the form:

$$0 = g_{i,t}(x), \text{ for } i = 1, 2,\ t > T, \quad (9)$$

where $g_{i,t}(x) = \tilde{g}_{i,t}(x) - \tilde{g}_{i,t-T}(x)$, and essentially the state x here only involves the equivalent reactance X_i.

1) Modified extended Kalman filter (MEKF): In this case, since the dynamic states are not involved, with the discretized model in (9), the extended Kalman filter for the modified system is given by

$$\hat{x}_k = \hat{x}_{k-1} - S_k^{-1} \nabla g_{i,k}(\hat{x}_{k-1}) g_{i,k}(\hat{x}_{k-1}), \quad (10a)$$
$$S_k = \lambda S_{k-1} + \nabla g_{i,k}(\hat{x}_{k-1}) \nabla g_{i,k}(\hat{x}_{k-1})^T, \quad (10b)$$

where λ can be viewed as a fading factor, k indicates the k^{th} step and $S_0 = 0$. Further information on the derivation of (10) can be found in [9], [10].

As illustrated in Example 2 below, the convergence property improves significantly; in other words, the convergence region of the initial states has been expanded substantially. In our system, due to the convex property of (8), according to Proposition 2 of [10], the initial state estimate can be set as an arbitrary value. However, when the initial state estimates are far from the correct value, the estimation likely fails to converge to the correct values. In order to address this issue, the iterated extended Kalman filter ([10], [11]) is introduced as described next.

2) Iterated extended Kalman filter (IEKF): The basic concept behind the iterated extended Kalman filter is to iteratively use multiple copies of the data set [10]; in other words, after n steps, the final estimates will be used as the initial state estimates and the extended Kalman filter processing will repeat from the beginning. The filter dynamics can be described by:

$$\hat{x}_{cn+k} = \hat{x}_{cn+k-1} - S_{cn+k}^{-1} \nabla g_{i,k}(\hat{x}_{cn+k-1}) g_{i,k}(\hat{x}_{cn+k-1}),$$
$$S_{cn+k} = \lambda S_{cn+k-1} + \nabla g_{i,k}(\hat{x}_{cn+k-1}) \nabla g_{i,k}(\hat{x}_{cn+k-1})^T,$$

where $c = 0, \cdots, C-1$; $k = 1, \cdots, n$.

The iterated extended Kalman filter can guarantee the convergence bias error approaches to zero, when the number of repetition C is large enough. However, the main drawback in IEKF is that a set of n measurements must be available before the estimation process can begin. Hence, it cannot proceed recursively as in a traditional Kalman filter.

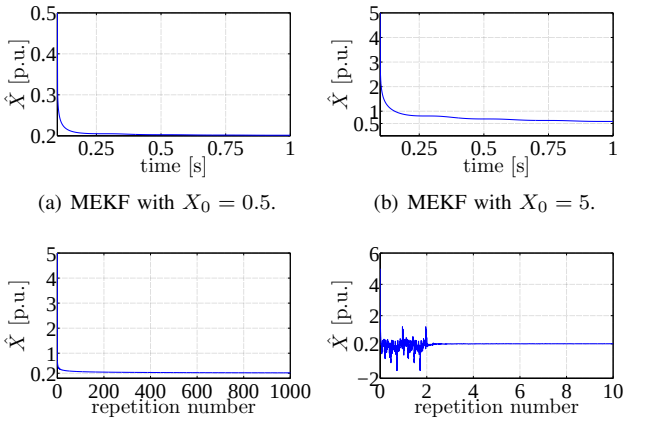

(a) MEKF with $X_0 = 0.5$. (b) MEKF with $X_0 = 5$.

(c) IEKF with $X_0 = 5$. (d) IEKF with adaptive fading factor and $X_0 = 5$.

Fig. 4: MEKF and IEKF.

We may further improve the performance of IEKF by setting the fading factor λ to a value smaller than one, leading to faster convergence rates than for $\lambda = 1$ [10]. However, for $\lambda = 1$, higher accuracy is obtained since it smooths the noises better by weighting all measurements equally. To take advantage of the trade-off between convergence rate and accuracy, we apply different values of λ in different iterations, with $\lambda < 1$ in earlier iterations and $\lambda = 1$ afterwards.

Example 2: Consider, again, the system discussed in Example 1. The MEKF and IEKF are applied to the measurement set. In Fig. 4(a), using MEKF, X_1 converges to the correct value (0.2 p.u.) even when the initial state is set to be 0.5, which is far from the correct value. However, when the initial state estimate is further from the correct value, (e.g., 5 p.u.), although MEKF still converges; convergence error occurs at the final state estimate. As shown in Fig. 4(b), the estimate of X at the last time step is above 0.5. Using IKEF, the estimates converge to the correct value as shown in Fig. 4(c), although many iterations are required for convergence. In Fig. 4(d), $\lambda = 0.8$ is applied in the first 2 iterations and the convergence rate is improved significantly over that shown in Fig. 4(c). ■

C. Filter Application

Within the context of this paper, according to the advantages and drawbacks of the different filters, we summarize the applications of different filters in different situations.

(i) In the beginning, since we have little information about the range of the states. IEKF should be applied to obtain the precise initial state estimates.

(ii) With the precise initial state estimates, on-line MEKF can be applied to recursively estimate the equivalent reactance in real time.

(iii) With equivalent reactance X_i known, the E_i and δ_i are readily obtained using Kirchhoff's voltage laws:

$$E_i \angle \delta_i = V_i \angle \theta_i + jX_i I_i \angle \gamma_i,\ i = 1, 2.$$

Then the stability margin, as well as the loadability

characteristics, can be evaluated by using (1). If the state variables in the state equations are of interest, the EKF with full model can be applied to estimate those states, such as the equivalent inertia.

IV. Case Study

In this section, we apply the methology described in the previous sections to analyze a two-area system with four generators and two loads. All the generator models include subtransient effects, exciters and governors. The transmission line of interest is the long tie line connecting two areas with relatively high reactance. Two PMUs are assumed to be set at the two terminals of this line to collect measurements. The MATLAB-based Power System Toolbox (PST) is utilized to simulate this system. This two-area system is a modification of one of the PST demonstration systems and the details and parameters can be found in [12]. In this study, the loads are changed randomly to inject small disturbance into the system. The time-varying loads obey the normal distribution with variance of 1 p.u. The voltage phasors, as well as the current phasors flowing are recorded and assumed to emulate as the PMU measurements.

In the base case, after injecting the load variation disturbance and applying the estimation method described in Section III, the angle difference across the line (i.e., $\theta_1 - \theta_2$) and the angle-across-system $(\delta_1 - \delta_2)$ are depicted in Fig. 5. In the first 0.5 s, the AAS value is missing because as mentioned in Section III-C initially a batch of measurements (the measurements from 0 to 0.5 s in this case) are needed to apply IEKF. As shown in Fig. 5(a), even $\theta_1 - \theta_2$ is less than 30 deg. The actual AAS has already been up to around 59 deg. Next we reduce both loads by 50%, the power flowing on the tie line is also reduced by 50%. Similarly, the angle-across-line and angle-across-system are depicted in Fig. 5(b). The AAS and corresponding stability margin in the two cases are listed in Table II. As we mentioned earlier, the power flow is proportional to the sine of the AAS. This is consistent with the numbers in the table, where the sine of the AAS in the base case is 0.86, while it is 0.42 when the system is 50% less loaded. On the other hand, since the SM is 0.14 for the base case, the maximum power flow should be equal to 116% (i.e., $1/(1 - \text{SM})$) of the power flow in the base case. To validate this, we increase the loads by the step of 1% and we find that 115% is the threshold over which the system fails to function. The closeness of 115% and 116% verifies the accuracy of this method.

V. Conclusions

In this paper, we proposed a framework to assess the operating transmission line loadability; particularly, we study the stability factor which limits the loadability. In this framework, we evaluate the stability margin by a function of the angle across the equivalent system; and subsequently, the line loadability can be easily assessed based on the current power flow and stability margin.

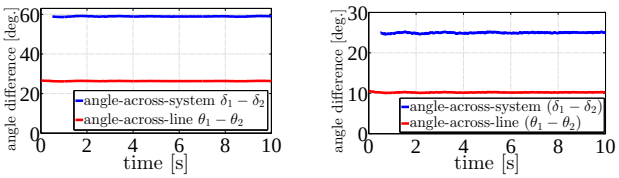

(a) Base case. (b) 50% less loaded case.

Fig. 5: Angle-across-line vs. angle-across-system.

TABLE II: Stability measures in two cases.

	Avg. AAS [deg.]	sin (AAS)	SM
Base Case	58.95	0.86	0.14
50% Less Loaded	24.96	0.42	0.58

The focus here was to obtain the equivalent two-area system model using synchrophasor measurements. To this end, we proposed the use of extended Kalman filtering to obtain the parameters of the equivalent model. We illustrated the advantages and drawbacks of different algorithms for extended Kalman filtering in several numerical examples.

References

[1] H. St.Clair, "Practical concepts in capability and performance of transmission lines," *Power Apparatus and Systems, Part III. Transactions of the American Institute of Electrical Engineers*, vol. 72, no. 2, pp. 1152–1157, 1953.

[2] R. Gutman, P. Marchenko, and R. Dunlop, "Analytical development of loadability characteristics for EHV and UHV transmission lines," *Power Apparatus and Systems, IEEE Transactions on*, vol. PAS-98, no. 2, pp. 606–617, 1979.

[3] R. Gutman, "Application of line loadability concepts to operating studies," *Power Systems, IEEE Transactions on*, vol. 3, no. 4, pp. 1426–1433, 1988.

[4] A. Phadke and J. Thorp, *Synchronized Phasor Measurements and Their Applications*. New York: Springer, 2008.

[5] J. Chow, A. Chakrabortty, L. Vanfretti, and M. Arcak, "Estimation of radial power system transfer path dynamic parameters using synchronized phasor data," *Power Systems, IEEE Transactions on*, vol. 23, no. 2, pp. 564 –571, May 2008.

[6] A. Chakrabortty, J. Chow, and A. Salazar, "A measurement-based framework for dynamic equivalencing of large power systems using WAMS," in *Innovative Smart Grid Technologies (ISGT), 2010*, Jan. 2010, pp. 1 –8.

[7] K. E. Reinhard, P. W. Sauer, and A. D. Domínguez-García, "On computing power system steady-state stability using synchrophasor data," in *2013 46th Hawaii International Conference on System Sciences (HICSS),*, 2013, pp. 1–8.

[8] M. Verhaegen and V. Verdult, *Filtering and System Identification: A Least Squares Approach*. Cambridge University Press.

[9] B. Bell and F. Cathey, "The iterated kalman filter update as a gauss-newton method," *Automatic Control, IEEE Transactions on*, vol. 38, no. 2, pp. 294–297, 1993.

[10] D. Bertsekas, "Incremental least squares methods and the extended kalman filter," *SIAM Journal on Optimization*, vol. 6, no. 3, pp. 807–822, 1996.

[11] A. Alessandri, M. Cuneo, S. Pagnan, and M. Sanguineti, "A recursive algorithm for nonlinear least-squares problems," *Computational Optimization and Applications*, vol. 38, no. 2, pp. 195–216, 2007.

[12] "Power system toolbox," http://www.eps.ee.kth.se/personal/vanfretti/pst.